Assessing the impact of valence math xmlns="http://www.w3.org/1998/Math/MathML">mrow>mi mathvariant="italic">sd/mi>/mrow>/math> neutrons and protons on fusion

Varinderjit Singh, J. Vadas, T. K. Steinbach, B. B. Wiggins, S. Hudan, and R. T. deSouza

Assessing the impact of valence *sd* neutrons and protons on fusion

Varinderjit Singh, J. Vadas, T. K. Steinbach, B. B. Wiggins, S. Hudan, and R. T. deSouza*

Department of Chemistry and Center for Exploration of Energy and Matter, Indiana University

2401 Milo B. Sampson Lane, Bloomington, Indiana 47408, USA

(Dated: May 12, 2021)

Experimental near-barrier fusion cross-sections for ^{17}F + ^{12}C are compared to the fusion excitation functions for ^{16,17,18}O, ^{19}F, and ^{20}Ne ions on a carbon target. Normalized or reduced fusion cross-sections are utilized in order to compare the different systems and account for the differing static size of the incident ions as well as changes in fusion barrier. Fusion excitation functions for the case of the mirror nuclei ^{17}F and ^{17}O with a single *sd* nucleon are compared. The ^{17}F data are also juxtaposed with nuclei involving multiple *sd* nucleons. Trends of the fusion cross-section above the barrier beyond the expected systematic behavior are observed. These trends are interpreted as the interplay of the *sd* protons and neutrons. The experimental data are also compared to a widely-used analytic model of near-barrier fusion, a time-dependent Hartree-Fock model, and coupled channels calculations.

PACS numbers: 21.60.Jz, 26.60.Gj, 25.60.Pj, 25.70.Jj

Nuclear fusion is a topic of considerable interest both from a fundamental perspective as well as in the field of nuclear astrophysics [1]. Nuclei just beyond a closed shell present a unique opportunity to probe the interplay of shell and collective effects on the fusion process. In particular, light nuclei just beyond the $1p_{1/2}$ shell, namely isotopes of oxygen, fluorine, and neon are good candidates for examination. In this work, the fusion of various isotopes of these elements with a carbon target at near-barrier energies is examined. The results of this work, which combines both stable and radioactive beams, points to the potential of low-energy beams at radioactive beam facilities [2, 3] for examining the impact of neutron-excess on fusion.

Addition of neutrons and protons just beyond the $1p_{1/2}$ shells of ^{16}O clearly changes both the matter and charge distributions of the nuclei. Theoretical calculations indicate that for a large neutron excess, e.g. ^{24}O as compared to ^{16}O, fusion with ^{16}O target is significantly enhanced [4]. The impact of adding just a few neutrons or protons beyond the $1p_{\frac{1}{2}}$ shell on fusion is less clear. With increased atomic or mass number, the fusion barrier and consequently the fusion cross-section is clearly impacted. We propose to go beyond these trivial systematic differences and examine the detailed differences in the fusion cross-section. A particularly interesting case to investigate is fusion of the nucleus ^{17}F which exhibits a proton-halo when in its $2s_{1/2}$ excited state [5]. It is presently unclear whether an increased radial extent results in a fusion enhancement or weak binding results in a decreased fusion cross-section. For the case of ^{17}F + ^{208}Pb, neither an enhancement nor a suppression of fusion was observed relative to ^{19}F + ^{208}Pb [6]. However, in the case of fusion with a large target nucleus, such as ^{208}Pb, the impact on fusion of adding two neutrons might be diminished. Recently, the fusion cross-section for ^{17}F

+ ^{12}C both at near-barrier energies [7] and higher energies [8] has been reported indicating that the low binding energy of ^{17}F and the halo properties of the low-lying first excited state do not affect the low-energy fusion cross-section. In this work we report an independent, higher statistics measurement of near barrier fusion for ^{17}F + ^{12}C. By comparing the present measurement with fusion induced by O, F, and Ne beams on ^{12}C the impact of adding a few protons and neutrons to the *sd* shell on the fusion cross-section is examined.

I. EXPERIMENTAL DETAILS

Discovery of halo nuclei, notably ^{11}Li [9, 10] was achieved through systematic examination of the interaction cross-sections for lithium isotopes. At high incident energy one expects the sudden approximation to be valid in describing the collision of the nuclei. Consequently, the nuclear densities do not have enough time to rearrange as the projectile and target nuclei come into contact. Thus, a measurement of the interaction cross-section at high energy probes the nuclear size and other geometrical features such as deformation, all of which are considered "static" [9]. Hence, the measured interaction cross-section, σ_I, provides a direct and effective measure of the extent of the matter distribution.

To better understand the change in the static size of the different nuclei considered in this work, we examine the interaction cross-sections measured at high energy. Presented in Table I are σ_I for O, F, and Ne nuclei with a carbon target [11] with the number of protons and neutrons in the *sd* shell indicated. The closure of the $1p_{\frac{1}{2}}$ with N=8 provides a natural reference from which to examine the impact made by the presence of a few nucleons in the *sd* shell. Addition of two neutrons to ^{16}O, ^{17}F, and ^{18}Ne increases the interaction cross-section by 50, 61, and 68 mb respectively. Addition of two protons to ^{16}O, i.e. ^{18}Ne, results in an increase of σ_I by 94 mb while in the

* desouza@indiana.edu

TABLE I. Interaction cross-sections for oxygen, fluorine, and neon nuclei with a carbon target at an E$\approx$ 900 A.MeV. Taken from [11].

$^{18}\text{Ne}^{2p0n}$	$^{20}\text{Ne}^{2p2n}$
σ_I=1076$\pm$25 mb	σ_I=1144$\pm$10 mb
$^{17}\text{F}^{1p0n}$	$^{19}\text{F}^{1p2n}$
σ_I=982$\pm$32 mb	σ_I=1043$\pm$24 mb
$^{16}\text{O}^{0p0n}$	$^{18}\text{O}^{0p2n}$
σ_I=982$\pm$6 mb	σ_I=1032$\pm$26 mb

case ^{18}O to ^{20}Ne, it increases by 112 mb. The difference in the interaction cross-section with the addition of two protons (94-112 mb) as compared to addition of two neutrons (50-68 mb) is presumably due to the repulsion of the two protons with the ^{16}O core. Such a difference is not captured by systematics which relate the radius of a nucleus to simply the mass number, A, suggesting the advantage of using σ_I to account for trivial size effects.

While the excitation function for fusion of ^{16,18}O, ^{19}F, and ^{20}Ne ions with a carbon target already exists, little or no data exists for ^{17}F+^{12}C or ^{18}Ne+^{12}C. The experiment was performed at the John D. Fox accelerator laboratory at Florida State University where a beam of ^{16}O ions accelerated to an energy of $\approx$4.5 MeV/A was incident on a deuterium gas cell. This cell served as a production target and was maintained at a pressure of 350 torr and a temperature of 77K. Ions of ^{17}F were produced via a (d,n) reaction. These ions were separated from the incident beam by the electromagnetic spectrometer RESOLUT [12]. The beam exiting the spectrometer consisted of both ^{17}F and residual ^{16}O ions necessitating identification of each ion on a particle-by-particle basis. The presence of both species allowed the simultaneous measurement of ^{16}O + ^{12}C and ^{17}F + ^{12}C providing a built-in reference measurement and comparison with the well-established fusion excitation function for ^{16}O + ^{12}C.

The setup used to measure fusion of fluorine and oxygen ions with carbon nuclei in this experiment is depicted in Fig. 1. Upon exiting the RESOLUT spectrometer particles traverse a thin foil (0.5 μm thick aluminized mylar) ejecting electrons in the process. These ejected electrons are accelerated and deflected from the beam axis onto the surface of a microchannel plate detector, MCP$_{RESOLUT}$, where they are amplified, producing a fast timing signal. The ions subsequently traverse a compact ionization chamber (CID), situated $\approx$3.5 m downstream of MCP$_{RESOLUT}$. In passing through this detector ions deposit an energy (ΔE) characterized by their atomic number (Z), mass number (A), and incident energy. Upon exiting CID the ions are incident upon a carbon foil which serves both as a secondary emission foil for MCP$_{TGT}$ as well as the target for the experiment. In order to maximize the production cross-section for ^{17}F, it was necessary to operate at high incident energy and keep the pressure of the deuterium production gas cell at a constant value. Consequently, in order to adjust
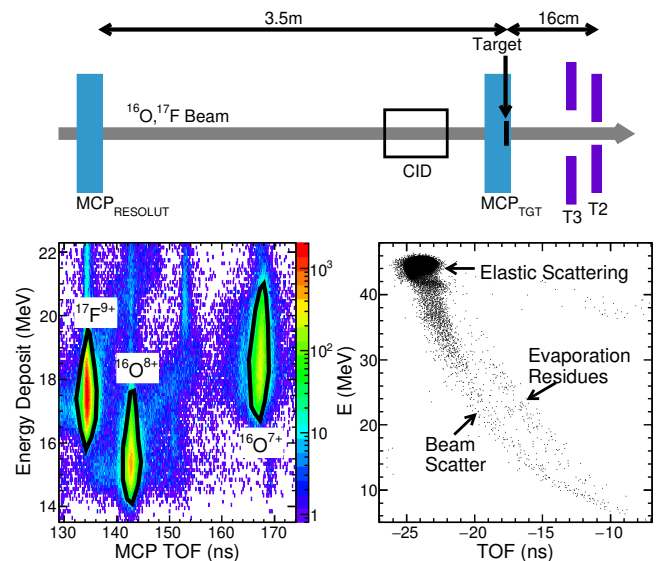

FIG. 1. (Color online) Schematic of the experimental setup along with a PID and ETOF spectra. Particle identification of the ^{17}F and ^{16}O ions incident on the target is displayed in the left plot. In the right plot a representative ETOF spectrum (selected on ^{17}F) used to identify evaporation residues (ER) at E$_{LAB}$=30.7 MeV.

the energy of the beam on target, the pressure in CID was adjusted. As the pressure in CID can be well controlled it provides a much more uniform degrader than a solid foil. To determine the energy of the beam incident on the target a silicon detector was periodically inserted just prior to the target. This provided a measure of the energy distribution of the ^{17}F and ^{16}O ions incident on the target. The width of the energy distribution for ^{17}F ions was between 400-500 keV and was principally determined by straggling in the deuterium gas cell, not CID. All the excitation functions have been corrected for the width of the energy distribution. Data were acquired at each energy incident on the target between $\approx$5 hours at the highest energy to 10-15 hours at the lower energies.

The two microchannel plate detectors together with CID permitted a ΔE-TOF measurement for each ion incident on the target. Measurement of the ΔE-TOF (Fig. 1) clearly shows three peaks corresponding to ^{17}F^{9+}, ^{16}O^{7+}, and ^{16}O^{8+} ions. The intensity of the ^{17}F beam incident on the target was 3-7 x 10^3 ions/s with a purity of 37%-54%.

Fusion of a ^{17}F (^{16}O) nucleus in the beam together with a ^{12}C nucleus in the target foil results in the production of an excited ^{29}P (^{28}Si) nucleus. For near-barrier collisions the excitation of the fusion product is relatively modest, E* $\approx$ 30-50 MeV. Emission of particles as the fusion product de-excites, deflects the evaporation residue (ER) from the beam direction. This deflection allows its detection and identification using two annular silicon detectors designated T2 and T3 that subtend the angular range $3.5° < \theta_{lab} < 25°$. Using the measured energy de-

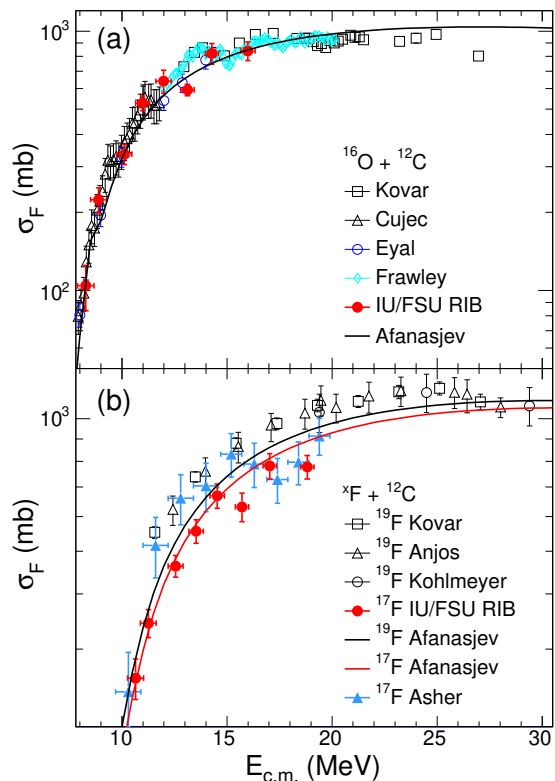FIG. 2. (Color online) Fusion excitation functions for ^{16}O + ^{12}C (top panel) and ^{17,19}F + ^{12}C (bottom panel). The predictions of an analytic fusion model [13] are indicated by the solid lines.

posit in the silicon detectors and the time-of-flight [14], ERs were cleanly distinguished from beam particles by their position in the ETOF spectrum as evident in Fig. 1 [15, 16].

The fusion cross-section, σ_F is extracted from the measured yield of evaporation residues through the relation $\sigma_F = N_{ER}/(\epsilon_{ER} \text{ x } t \text{ x } N_I)$ where N_I is the number of beam particles of a given type incident on the target, t is the target thickness, ϵ_{ER} is the detection efficiency, and N_{ER} is the number of evaporation residues detected. The number N_I is determined by counting the particles with the appropriate time-of-flight between the two microchannel plates that additionally have the correct identification in the ΔE-TOF map depicted in Fig. 1. The target thickness, t, for the foil used is determined by the manufacturer to be 105 ± 0.5 μg/cm^2 using an optical transmittance measurement. The number of detected residues, N_{ER}, is determined by summing the number of detected residues clearly identified by the ETOF technique as shown in Fig. 1 [16]. The uncertainty in accurately determining the number of ERs is included in the error analysis. To determine the total fusion cross section it is necessary to know the geometric efficiency, ϵ_{ER}, of the experimental setup. The efficiency was determined by using a statistical model, evapOR [17], which simulates the decay of a compound nucleus using a Hauser-

Feshbach approach. This program, derived from PACE2 [18], was optimized for the statistical decay of light nuclei. By calculating the fraction of the evaporation residues that lie within the detector acceptance, the geometric efficiency of the experimental setup is obtained. The detection efficiency varied from ≈81% at the highest incident energies measured to ≈85% at the lowest incident energy due to the changing kinematics of the reaction with an associated uncertainty of approximately 5%. Comparison with a more widely-used statistical model PACE4 [18] predicts essentially the same efficiencies. Due to the low detection thresholds of the ETOF approach this detection efficiency reflects the coverage in the center-of-mass frame of the annular silicon detectors. Using the efficiency together with the measured evaporation residue yield, the total fusion cross section is extracted. Since the MCP efficiency affects both the counting of the total number of beam particles and the number of evaporation residues, it does not impact the measured total fusion cross section. The accuracy of the target thickness and the efficiency calculations is validated by the accurate description of the fusion excitation function for ^{16}O + ^{12}C presented in Fig. 2.

TABLE II. Fusion cross-sections for ^{17}F and ^{16}O on ^{12}C

$E_{c.m.}$ (MeV)	σ (mb)	$E_{c.m.}$ (MeV)	σ (mb)
	^{17}F		^{16}O
18.82±0.32	777±47	16.0±0.34	839±69
17.03±0.32	781±51	14.3±0.30	821±76
15.71±0.32	630±47	13.1±0.32	594±30
14.53±0.34	668±42	12.0±0.37	642±66
13.53±0.35	555±34	11.0±0.33	527±34
12.55±0.36	463±26	10.1±0.36	336±30
11.26±0.37	343±25	8.9±0.38	224±25
10.65±0.38	258±27	8.3±0.39	104±21

II. RESULTS AND DISCUSSION

Depicted in Fig. 2 are the measured excitation functions for fusion of ^{16}O and ^{17}F ions with a carbon target. The data are also presented in tabular form in Table II. With the experimental technique used, both the ^{16}O + ^{12}C and ^{17}F + ^{12}C excitation functions are simultaneously measured. In the top panel, for ^{16}O, one observes the good agreement of this measurement, depicted as the solid (red) circles, with the experimental cross-sections reported in the literature [20–23]. This agreement is strong evidence that the measurement of the fusion excitation function for ^{17}F + ^{12}C is robust. In the lower panel of Fig. 2 the measured cross-sections for ^{17}F+^{12}C (solid red circles) are presented along with

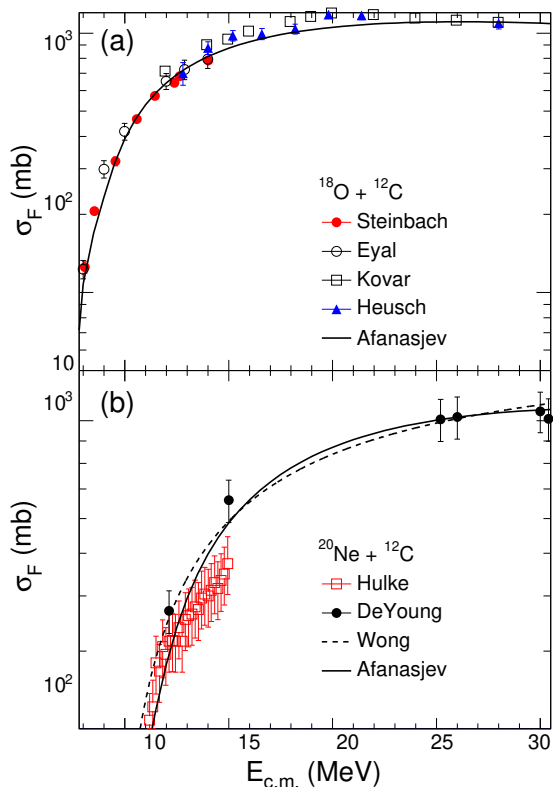FIG. 3. (Color online) Fusion excitation functions for ^{18}O+^{12}C (top panel) and ^{20}Ne+^{12}C (bottom panel) together with the predictions of the analytic model [13]. The fit of the ^{20}Ne data by a one-dimensional barrier-penetration model [19] is depicted by the dashed line.

the excitation function for ^{19}F+^{12}C. The multiple measurements for ^{19}F [22, 24, 25] are in agreement within the measurement uncertainties. As might be expected naively by the reduction of two neutrons, the ^{17}F-induced fusion of this measurement exhibits a lower cross-section than ^{19}F for all energies shown. The measured excitation functions are compared with the predictions of an analytic model based on a parameterization of the Sao Paulo potential model coupled with a barrier penetration formalism [13, 26, 27]. This model which has parameterized a large number of reactions for low and mid-mass systems is a useful tool for network simulations in the near-barrier regime. Despite having several fitted parameters, the analytic model has no adjustable parameters and thus serves as a useful benchmark of the expected systematic behavior. The cross-sections predicted by this model are depicted in Fig. 2 as the solid lines. In the case of the ^{16}O fusion the analytic model provides a reasonable description of the overall behavior of the excitation function. The failure of the analytic model to reproduce the resonances is unsurprising as it assumes a smooth, structureless barrier. For the fluorine isotopes, while the excitation function for ^{17}F is reasonably described, the experimental excitation function for ^{19}F is clearly underpredicted in the energy range measured. Nonetheless,

the analytic model does predict an increase in the cross-section associated with the presence of the two additional neutrons in ^{19}F as compared to ^{17}F.

Also presented in Fig. 2 is the excitation function for ^{17}F + ^{12}C recently measured by Asher (solid blue triangles) [7]. The statistical uncertainties of the Asher measurement are significantly larger than those of the present measurement. As importantly, the Asher measurement has significantly larger uncertainty in the energy. Even considering the uncertainties of both excitation functions it is clear that the Asher excitation function reports larger cross-sections or is shifted to lower energies as compared to the present measurement. Surprisingly, the excitation function measured by Asher for $E_{c.m.} \leq 15$ MeV is essentially consistent with the excitation function for ^{19}F. This result would imply that the removal of two neutrons from ^{19}F makes a negligible difference in both the barrier and the size of the fusing system. Such a result is inconsistent with the analytic model results which describes the expected systematic behavior.

The excitation functions for fusion of ^{18}O and ^{20}Ne nuclei with carbon are shown in Fig. 3. While good agreement is observed for the various ^{18}O datasets, [16, 21, 22, 28], in the case of ^{20}Ne, for 12 MeV $\leq E_{c.m.} \leq 15$ MeV a discrepancy exists between the measurements of Hulke [29] and deYoung [30]. This discrepancy at $E_{c.m.} \sim 15$ MeV is larger than the reported uncertainties by both experimental measurements. Moreover, the shape of the excitation function determined by Hulke [29] deviates from the behavior of a smooth barrier as indicated by the analytic model [13]. The Hulke data [29] for $E_{c.m.} \leq 11$ MeV and the deYoung data [30] can be described by a one-dimensional barrier penetration model [19] as indicated by the dashed line in Fig. 3.

TABLE III. Bass barriers (in MeV) for O, F, and Ne isotopes

	^{16}O	^{18}O	^{17}F	^{19}F	^{20}Ne
V_B	7.95	7.78	8.95	8.77	9.74

In order to appropriately compare all the fusion excitation functions for these light nuclei, we scale the fusion cross-section by the interaction cross-section, σ_I, presented in Table I. In addition, the trivial effect of the different barriers is accounted for by examining the normalized cross-section, σ_F/σ_I, as a function of the above-barrier energy, $E_{c.m.}$-V_B. The value of the barrier, V_B, is taken from the Bass model [31]. The barriers calculated in this model are presented in Table III. Addition of two neutrons to ^{17}F, namely ^{19}F, results in a barrier reduction of 180 keV, comparable to the reduction of 170 keV observed in going from ^{16}O to ^{18}O. Addition of a proton to ^{16}O increases the barrier by 1.0 MeV but addition of a second proton only results in a further increase of $\approx$0.8 MeV. The uncertainties shown in the normalized cross-section reflect the uncertainties in both σ_F and σ_I. This presentation allows one to investigate differences between the nuclei shown after effectively eliminating systematic

differences in the static size and barrier. Comparison of all the excitation functions in Fig. 4 yields some interesting results. In Fig. 4a one observes that for $(E_{c.m.}-V_B) \leq 9$ MeV, the normalized cross-sections for ^{16}O and ^{18}O are relatively comparable. The prominent resonance structure for ^{16}O-induced fusion is absent in the case of ^{18}O. Above 9 MeV one observes that the normalized cross-section for ^{18}O exceeds that of ^{16}O. This increase in the normalized cross-section indicates the impact of the two sd neutrons on the fusion cross-section *over and above the increase in the static size*. In further understanding the role of sd valence nucleons on fusion, we elect to choose ^{18}O as our reference. The absence of strong, sharp resonance structures in the ^{18}O reaction supports this choice. To facilitate the use of ^{18}O as a reference we have described the data by the smooth curve depicted in Fig. 4a. This curve corresponds to a third-order polynomial fit to the normalized cross-sections for ^{18}O and simply serves as an adequate representation of the ^{18}O data in Fig. 4b.

Presented in Fig. 4b are the normalized excitation functions for ^{19}F, ^{20}Ne, and ^{17}F in comparison to ^{18}O. Within the measurement uncertainties the ^{19}F data manifests the same normalized cross-section as the ^{18}O. However, there is a subtle indication that the normalized cross-section for ^{19}F appears to be systematically slightly lower than that of ^{18}O for $(E_{c.m.}-V_B) \geq 9$ MeV. The $\langle \sigma_F/\sigma_I \rangle$ in this energy interval is 1.11 ± 0.04 for ^{18}O and 1.06 ± 0.07 for ^{19}F. This comparison between ^{18}O and ^{19}F is complicated by the presence of the unpaired proton in ^{19}F.

Examination of the normalized cross-section for ^{20}Ne is more telling. For all energies measured, the ^{20}Ne normalized cross-section is lower than that of both ^{18}O and ^{19}F. Unfortunately, lack of data between $\sim$5 MeV$\leq$(E$_{c.m.}$-V$_B$)$<$15 MeV prevents a better characterization of this excitation function. The normalized cross-sections for ^{17}F observed in this work are decreased as compared to the cross-sections for ^{19}F for the entire energy range measured. This decreased value for ^{17}F as compared to ^{19}F is qualitatively consistent with the trend observed for ^{18}O and ^{16}O.

To investigate the interaction of the valence protons on the valence neutrons we have performed Relativistic Mean Field (RMF) calculations of the neutron and proton density distributions of light nuclei. In examining the proton and neutron density distributions for neutron-rich carbon nuclei from these RMF calculations, one observes that with increasing neutron number not only does the tail of the neutron density distribution extend further out but despite a constant number of protons, the proton density distribution is slightly extended [32]. This interaction between valence protons and neutrons is also reflected in the one proton separation energies of ^{16}O,^{18}O, and ^{20}O which are 12.1, 15.9, and 19.3 MeV respectively.

Based upon these calculations we hypothesize that the slight decrease in the cross-section for ^{19}F as compared to ^{18}O could reflect the attraction of the sd proton on
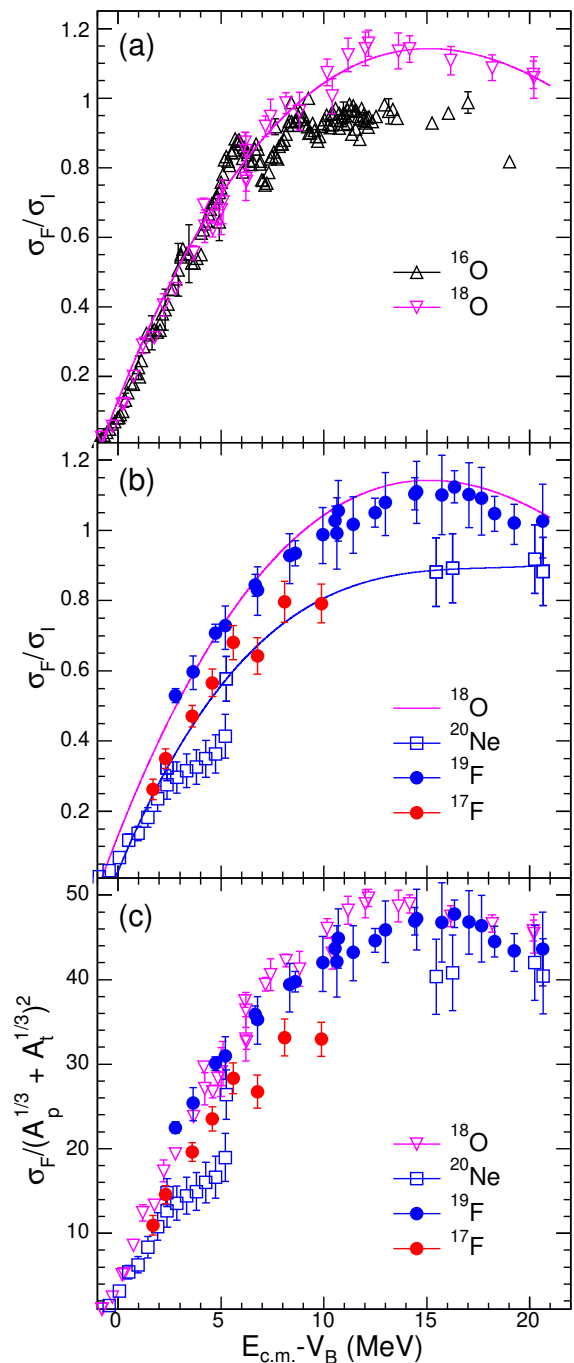

FIG. 4. (Color online) Comparison of the normalized and reduced excitation functions for fusion of ^{16}O and ^{18}O ions (top panel) and ^{18}O, ^{20}Ne, ^{19}F, and ^{17}F ions (lower panels) on a carbon target. The line through the ^{20}Ne data simply serves to guide the eye.

the two sd neutrons resulting in a reduction of the fusion probability. The lower cross-sections for ^{20}Ne as compared to ^{18}O and ^{19}F is similarly consistent with the attraction of the two sd protons on the two sd neutrons and the consequent suppression of fusion. It should be appreciated that the explanation of these observations is at a
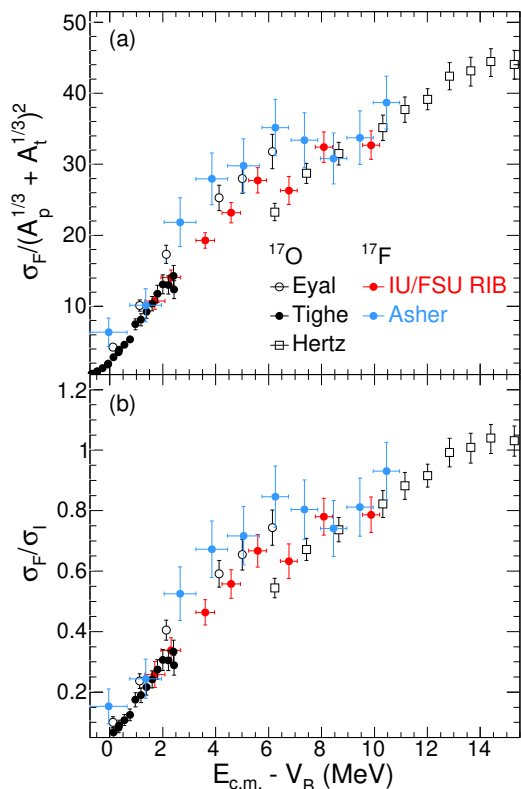
FIG. 5. (Color online) Comparison of the reduced fusion excitation function and normalized excitation function for the mirror nuclei ^{17}F and ^{17}O with a ^{12}C target.

qualitative level and a more quantitative description will require more sophisticated theoretical calculations which include nuclear structure.

To assess the sensitivity of our results to the use of the interaction cross-section, σ_I, as a reference, we have calculated the reduced cross-section as $\sigma_F/(A_P^{\frac{1}{3}}+A_T^{\frac{1}{3}})^2$ where A_P and A_T are the mass number of the projectile and target nuclei respectively. While more sophisticated prescriptions for the reduced cross-section have been utilized in comparing dissimilar systems, given the similarity of the systems compared in this work this simple scaling is appropriate [33]. Examining the dependence of this quantity on $(E_{c.m.}-V_B)$ in Fig. 4c reveals that although the reduced cross-section for ^{20}Ne lies closer to that of ^{19}F, the trends observed in Fig. 4b remain the same indicating the robustness of the observations.

Examination of mirror nuclei is a powerful tool in understanding nuclear structure. The mirror nucleus of ^{17}F is ^{17}O in which the valence sd proton is replaced by a neutron. We therefore compare the fusion excitation functions for ^{17}F + ^{12}C with ^{17}O + ^{12}C in Fig. 5a. For the reaction ^{17}O + ^{12}C, three datasets [21, 34, 35] span the interval from sub-barrier energies to 14 MeV above the barrier. Significant differences are apparent between these three measurements. At the highest energy measured by Tighe, the measurement of Eyal predicts a cross-section that is approximately 30% larger. In contrast, at

$(E_{c.m.}-V_B) \sim 6.5$ MeV Hertz et al. report a cross-section that is significantly lower than that of Eyal. This disparity between the reported cross-sections is puzzling. Superimposed on the ^{17}O data is the present ^{17}F measurement. It is interesting that the low energy points are in good agreement with Tighe while the high energy points (within uncertainties) are in agreement with Hertz. Moreover there is an indication of a supression in the cross-section at $(E_{c.m.}-V_B) \sim 6.5$ MeV. This agreement of the reduced cross-section for ^{17}F and ^{17}O suggests that for the case of a single sd nucleon, after the difference in barrier is accounted for, it does not matter if the valence nucleon is a proton or a neutron. The supression of the cross-section at $(E_{c.m.}-V_B) \sim 6.5$ MeV is reminiscent of the drop in normalized cross-section for ^{16}O at $(E_{c.m.}-V_B) \sim 6$ MeV which is attributable to resonances.

It is interesting to speculate on the cross-section supression evident in the ^{17}F and ^{17}O excitation functions at $(E_{c.m.}-V_B) \sim 6.5$ MeV. If one considers the limit in which the valence sd nucleon couples weakly to the doubly closed shell ^{16}O core, the structure effects observed in the ^{16}O excitation function should be only slightly altered. Stronger coupling would act to mitigate the resonance features in the excitation function. The absence of significant resonance structure in the case of ^{18}O thus indicates a stronger coupling of the two sd neutrons to the ^{16}O core than the lone sd neutron in ^{17}O. These expectations are qualitatively in agreement with the one neutron separation energies for ^{17}O and ^{18}O of 4.143 and 8.045 MeV respectively.

Also presented in Fig. 5a are the data from Asher. These data exhibit a significantly larger reduced cross-section in comparison to ^{17}O. Presented in Fig. 5b are the normalized cross-sections where the interaction cross-section, σ_I, has been used instead of the simple $A^{\frac{1}{3}}$ systematics. The same trends observed in Fig. 5a are also observed in this case although the error bars are larger due to the uncertainties associated with σ_I.

These observations for the fusion of light sd nuclei can be summarized as follows. In the case of a single sd nucleon the reduced fusion cross-section is insensitive to the identity of the nucleon. However, the fusion cross-section is enhanced by the presence of multiple sd neutrons. This increased cross-section is suppressed by the presence of multiple sd protons. It should be stressed that these changes in the fusion cross-section relative to the barrier are beyond the systematic changes expected. It is clear that further experimental data, particularly in the case of ^{20}Ne, ^{17}O, and ^{17}F would be extremely useful.

To investigate the role of dynamics in the ^{17,19}F + ^{12}C reaction we performed time-dependent Hartree Fock calculations. On general grounds the TDHF approach is well-suited to describing the large-amplitude collective motion associated with fusion. Artificial symmetry restrictions are eliminated by performing the TDHF calculations on a 3D cartesian grid [36]. Recent calculations [37] have provided a good description of above-
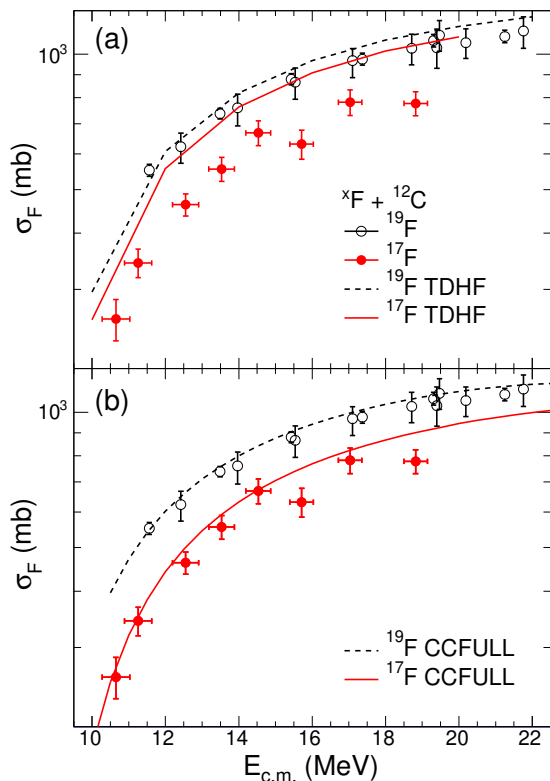
FIG. 6. (Color online) Comparison of the fusion excitation function for ^{17,19}F+^{12}C with the predictions of a TDHF model (panel a) and CCFULL (panel b).

barrier fusion data [38, 39]. The TDHF calculations were performed by initiating collisions for increasing impact parameters in steps of 0.01 fm until the maximum impact parameter for fusion is reached. Calculations were performed using the Sky3D model [40], with a SV-bas interaction with DDDI pairing. It should be noted that pairing significantly impacts the fusion cross-section in TDHF [16] emphasizing the need for its accurate description. The results of the TDHF calculations for ^{17}F and ^{19}F are depicted in Fig. 6a as the solid and dashed lines respectively. While the model provides a reasonable description of the ^{19}F data, the ^{17}F cross-sections are over-predicted. It should be noted that TDHF calculations often slightly overpredict the above-barrier cross-sections due to their neglect of breakup processes, complicating direct comparison of the cross-section. Nonetheless, it is noteworthy that the difference between ^{19}F and ^{17}F observed experimentally is not reproduced.

Coupled-channels calculations [41, 42] have been performed to assess the relative importance of the ground and excited states on the fusion cross-section. Results of CCFULL calculations [43] in which only the ground state of both target and projectile nuclei is considered are presented in Fig. 6b. A reasonable description of both excitation functions is achieved. Inclusion of excited states acts to increase the cross-section slightly, though primarily at sub-barrier energies. The limited impact of excited

states on fusion of ^{17}F in this near-barrier regime is consistent with other measurements [6, 7]. This description of the measured cross-sections corresponds to a potential in CCFULL with R_B= 7.89 fm, V_B=9.17 MeV, and $\hbar\omega$=3.36 MeV for ^{17}F and R_B= 8.42 fm, V_B=8.58 MeV, and $\hbar\omega$=2.94 MeV for ^{19}F. While the limited span of the experimental data does not permit a reliable extraction of $\hbar\omega$, the trend of increasing R_B and decreasing V_B with the addition of two neutrons is qualitatively understandable reflecting the increased nuclear interaction. These barriers can be compared to the Bass barriers presented in Table III. Although the magnitude and trends of the barriers in CCFULL is in rough agreement with the Bass model, some differences are observed. In the case of ^{17}F the CCFULL barrier is larger than the Bass barrier, 9.17 MeV as compared to 8.95 MeV. In contrast, for ^{19}F the CCFULL barrier is smaller, 8.58 MeV as compared to 8.77 MeV for Bass.

III. SUMMARY

Systematic comparison of the fusion excitation functions for isotopes of O, F, and Ne nuclei with a carbon target can be used to examine the impact of valence sd protons and neutrons on fusion. After accounting for differences in the static size of the incident nuclei and systematic changes in the fusion barrier, similarities and differences are noted between fusion of ^{17}O, ^{18}O, ^{17}F, ^{19}F, and ^{20}Ne with a carbon target. For the mirror nuclei ^{17}O and ^{17}F with just a single sd nucleon, the identity of the nucleon does not impact the reduced fusion cross-section after the trivial difference in Coulomb barrier is accounted for. The cases of multiple sd nucleons are more interesting. Although the reduced cross-section for ^{17}F is less than that of ^{19}F for all energies measured, at energies about 5 MeV above the barrier the reduced cross-section for ^{17}F is markedly less as compared to ^{19}F. This decrease is similar to the one observed for ^{16}O as compared to ^{18}O. The observed trend can be interpreted as the influence of multiple sd protons and neutrons on the reduced cross-section. In this framework, at energies upto 20 MeV above the barrier the presence of multiple valence sd neutrons acts to increase the effective size of the system that fuses *above the increase in the static size*. Both the ^{16}O/^{18}O and ^{17}F/^{19}F manifest this behavior. Comparison of a nucleus with sd protons and neutrons to one with sd neutrons alone indicates that the presence of the sd protons results in a decrease of the effective size. This behavior is interpreted as the strong interaction between the sd protons and the sd neutrons. It should be emphasized that this explanation of the trends noted is qualitative and a quantitative description which requires an accurate description of pairing effects is not yet available. Both a widely-used analytic model of fusion and a state-of-the-art dynamical model were used to investigate the systematic behavior expected. While both models predict a decrease in the cross-section with

removal of *sd* neutrons, the magnitude of the observed reduction in the fusion cross-section for ^{17}F as compared to ^{19}F is not reproduced. Coupled-channels calculations which consider only the ground state nuclei are able to reproduce the measured excitation functions despite the presence of the low-lying $2s_{1/2}$ proton-halo state. This initial observation of the sensitive interplay of valence neutrons and protons in the fusion of *sd* shell nuclei motivates further high-quality measurements of fusion for neutron-rich light nuclei. A new generation of radioactive beam facilities [2, 3], and in particular the availability of low-energy reaccelerated beams, provides an unprecedented opportunity to explore this topic and improve our understanding of low-density nuclear matter.

[1] B. B. Back, H. Esbensen, C. L. Jiang, and K. E. Rehm, Rev. Mod. Phys. **86**, 317 (2014).
[2] GANIL, Grand Accélérateur National d'Ions Lourds, Caen, France.
[3] FRIB, Facility for Rare Isotope Beams, Michigan State University, USA.
[4] A. S. Umar, V. E. Oberacker, and C. J. Horowitz, Phys. Rev. C **85**, 055801 (2012).
[5] R. Morlock, R. Kunz, A. Mayer, M. Jaeger, A. Mller, J. W. Hammer, P. Mohr, H. Oberhummer, G. Staudt, and V. Klle, Phys. Rev. Lett. **79**, 3837 (1997).
[6] K. E. Rehm, H. Esbensen, C. L. Jiang, B. B. Back, F. Borasi, B. Harss, R. V. F. Janssens, V. Nanal, J. Nolen, R. C. Pardo, M. Paul, P. Reiter, R. E. Segel, A. Sonzogni, J. Uusitalo, and A. H. Wuosmaa, Phys. Rev. Lett. **81**, 3341 (1998).
[7] B. W. Asher, S. Almaraz-Calderon, V. Tripathi, K. W. Kemper, L. T. Baby, N. Gerken, E. Lopez-Saavedra, A. B. Morelock, J. F. Perello, and I. Wiedenhover, Phys. Rev C **103**, 044615 (2021).
[8] L. Hu, Y. Song, and H. Liu, Nucl. Phys. A **1009**, 122167 (2021).
[9] I. Tanihata *et al.*, Phys. Lett. B **160**, 380 (1985).
[10] I. Tanihata, H. Hamagaki, O. Hashimoto, Y. Shida, N. Yoshikawa, K. S. O. Yamakawa, T. Kobayashi, and N. Takahashi, Phys. Rev. Lett. **55**, 2676 (1985).
[11] A. Ozawa, T. Suzuki, and I. Tanihata, Nucl. Phys. A **693**, 32 (2001).
[12] I. Wiedenhöver *et al.*, in *Fifth International Conference on Fission and Properties of Neutron-rich Nuclei*, edited by J. Hamilton and A. Ramayya (World Scientific, 2012) p. 144.
[13] A. V. Afanasjev, M. Beard, A. I. Chugunov, M. Wiescher, and D. G. Yakolev, Phys. Rev. C **85**, 054615 (2012).
[14] R. T. deSouza *et al.*, Nucl. Instr. Meth. A **632**, 133 (2011).
[15] T. K. Steinbach *et al.*, Nucl. Instr. Meth. A **743**, 5 (2014).
[16] T. K. Steinbach, J. Vadas, J. Schmidt, C. Haycraft, S. Hudan, R. T. deSouza, L. T. Baby, S. A. Kuvin, I. Wiedenhöver, A. S. Umar, and V. E. Oberacker, Phys. Rev. C **90**, 041603(R) (2014).

[17] N. G. Nicolis and J. R. Beene, (unpublished) (1983).
[18] A. Gavron, Phys. Rev C **21**, 230 (1980).
[19] C. Y. Wong, Phys. Rev. Lett. **31**, 766 (1973).
[20] B. Cujec and C. Barnes, Nucl. Phys. A **266**, 461 (1976).
[21] Y. Eyal, M. Beckerman, R. Chechik, Z. Fraenkel, and H. Stocker, Phys. Rev. C **13**, 1527 (1976).
[22] D. G. Kovar *et al.*, Phys. Rev. C **20**, 1305 (1979).
[23] A. D. Frawley, N. R. Fletcher, and L. C. Dennis, Phys. Rev. C **25**, 860 (1982).
[24] B. Kohlmeyer, W. Pfeffer, and F. Puhlhofer, Nucl. Phys. A **292**, 288 (1977).
[25] R. Anjos *et al.*, Phys. Rev. C **42**, 354 (1990).
[26] M. Beard, A. V. Afanasjev, L. C. Chamon, and L. Gasques, Atomic Data and Nuclear Data Tables **96** (2010), 10.1016/j.adt.2010.02.005.
[27] D. G. Yakolev, M. Beard, L. R. Gasques, and M. Wiescher, Phys. Rev. C **82**, 044609 (2010).
[28] B. Heusch, C. Beck, J. P. Coffin, P. Engelstein, R. M. Freeman, G. Guillaume, F. Haas, and P. Wagner, Phys. Rev. C **26**, 542 (1982).
[29] G. Hulke, C. Rolfs, and H. Trautvetter, Z. Physik A **297**, 161 (1980).
[30] P. A. deYoung, J. J. Kolata, R. C. Luhn, R. E. Malmin, and S. N. Tripathi, Phys. Rev. C **25**, 1420 (1982).
[31] R. Bass, *Nuclear Reactions with Heavy Ions* (Springer Verlag, 1980).
[32] R. deSouza, V. Singh, S. Hudan, Z. Lin, and C. Horowitz, (2020), arXiv:2007.11406.
[33] L. F. Canto, D. R. M. Junior, P. R. S. Gomes, and J. Lubian, Phys. Rev C **92**, 014626 (2015).
[34] A. Hertz, H. Essel, H. J. Korner, K. E. Rehm, and P. Sperr, Phys. Rev C **18**, 2780 (1978).
[35] R. J. Tighe, J. J. Kolata, and M. Belbot, Phys. Rev C **47**, 2699 (1993).
[36] A. S. Umar and V. E. Oberacker, Phys. Rev. C **73**, 054607 (2006).
[37] K.-H. Kim, T. Otsuka, and P. Bonche, Journal of Physics G: Nuclear and Particle Physics **23**, 1267 (1997).
[38] C. Simenel and B. Avez, Int. Jou. of Mod. Phys. E **17**, 31 (2008).

[39] C. Simenel, A. Umar, K. Godbey, M. Dasgupta, and D. Hinde, Phys. Rev. C **95**, 031601(R) (2017).

[40] B. Schuetrumpf, P.-G. Reinhard, P. D. Stevenson, A. S. Umar, and J. A. Maruhn, Computer Physics Communications **229**, 211 (2018).

[41] C. Dasso, S. Landowne, and A. Winther, Nucl. Phys. A **405**, 381 (1983).

[42] H. Esbensen, Phys. Rev C **77**, 054608 (2008).

[43] K. Hagino, N. Rowley, and A. T. Kruppa, Comput. Phys. Commun. **123**, 143 (1999).